การตรึงออสติโอพอนทินจากพืชบนเซลลูโลสเมมเบรนจากแบคทีเรียสำหรับการสร้างเนื้อเยื่อกระดูกใหม่

นางสาวณิชาภา กลิ่นธูปธำรง

วิทยานิพนธ์นี้เป็นส่วนหนึ่งของการศึกษาตามหลักสูตรปริญญาวิทยาศาสตรมหาบัณฑิต
สาขาวิชาปิโตรเคมีและวิทยาศาสตร์พอลิเมอร์
คณะวิทยาศาสตร์ จุฬาลงกรณ์มหาวิทยาลัย
ปีการศึกษา 2559

IMMOBILIZATION OF PLANT-DERIVED OSTEOPONTIN ON BACTERIAL CELLULOSE MEMBRANE FOR BONE TISSUE REGENERATION

Miss Nichapa Klinthoopthamrong

A Thesis Submitted in Partial Fulfillment of the Requirements
for the Degree of Master of Science Program in Petrochemistry and Polymer Science
Faculty of Science
Chulalongkorn University
Academic Year 2016

Thesis Title	IMMOBILIZATION OF PLANT-DERIVED OSTEOPONTIN ON BACTERIAL CELLULOSE MEMBRANE FOR BONE TISSUE REGENERATION
By	Miss Nichapa Klinthoopthamrong
Field of Study	Petrochemistry and Polymer Science
Thesis Advisor	Associate Professor Voravee Hoven, Ph.D.
Thesis Co-Advisor	Professor Prasit Pavasant, Ph.D.

Accepted by the Faculty of Science, Chulalongkorn University in Partial Fulfillment of the Requirements for the Master's Degree

.....Dean of the Faculty of Science
(Associate Professor Polkit Sangvanich, Ph.D.)

THESIS COMMITTEE

.....Chairman
(Professor Pattarapan Prasassarakich, Ph.D.)

.....Thesis Advisor
(Associate Professor Voravee Hoven, Ph.D.)

.....Thesis Co-Advisor
(Professor Prasit Pavasant, Ph.D.)

.....Examiner
(Assistant Professor Varawut Tangpasuthadol, Ph.D.)

.....External Examiner
(Assistant Professor Punnama Siriphannon, D.Eng.)

ณิชาภา กลิ่นธูปธำรง : การตรึงออสติโอพอนทินจากพืชบนเซลลูโลสเมมเบรนจากแบคทีเรียสำหรับการสร้างเนื้อเยื่อกระดูกใหม่ (IMMOBILIZATION OF PLANT-DERIVED OSTEOPONTIN ON BACTERIAL CELLULOSE MEMBRANE FOR BONE TISSUE REGENERATION) อ.ที่ปรึกษาวิทยานิพนธ์หลัก: รศ. ดร.วรวีร์ โฮเว่น, อ.ที่ปรึกษาวิทยานิพนธ์ร่วม: ศ. ทพ. ดร.ประสิทธิ์ ภวสันต์, 39 หน้า.

เซลลูโลสเมมเบรนจากแบคทีเรียหรือบีซี (bacterial cellulose; BC) เมมเบรน เป็นวัสดุที่มีศักยภาพในการพัฒนาไปเป็นแผ่นกั้นเนื้อเยื่อ (GTR membrane) เนื่องจาก มีความแข็งแรงเชิงกลและมีความเข้ากันได้ทางชีวภาพและยังมีพื้นผิวที่ง่ายต่อการดัดแปรหมู่ฟังก์ชัน ในงานวิจัยนี้เลือกตรึงออสติโอพอนทินหรือโอพีเอ็นที่ผลิตจากพืช (plant-produced osteopontin; pOPN) บนพื้นผิวของบีซีเมมเบรนเพื่อส่งเสริมการยึดเกาะและกระตุ้นการแปรสภาพไปเป็นเซลล์กระดูก พอลิเมอร์บรัชของพอลิอะคริลิกแอซิด (poly(acylic acid); PAA) จะถูกกราฟต์ลงบนบีซีเมมเบรน โดยอาศัยปฏิกิริยาพอลิเมอไรเซชันริเริ่มจากพื้นผิวผ่านกลไกแบบ Reversible Addition-Fragmentation Chain Transfer (RAFT) จากนั้นจึงตรึง pOPN ลงบนบีซีเมมเบรนผ่านปฏิกิริยาแอมิเดชันระหว่างหมู่คาร์บอกซิลของ PAA และหมู่แอมิโนของ pOPN ยืนยันความสำเร็จในการดัดแปรพื้นผิวแต่ละขั้นตอนด้วยเทคนิค ATR-FTIR และ XPS วิเคราะห์สัณฐานวิทยาพื้นผิวของบีซีเมมเบรนด้วยเทคนิค FE-SEM และ AFM วิเคราะห์ปริมาณ pOPN ที่ตรึงบนเมมเบรนด้วยเทคนิค ELISA assay ทดสอบการตอบสนองทางชีวภาพของเซลล์เอ็นยึดปริทันต์ต่อบีซีเมมเบรนที่กราฟต์ด้วย PAA และตรึง pOPN เปรียบเทียบกับโอพีเอ็นทางการค้าที่ผลิตจากเซลล์เลี้ยงลูกด้วยนม ผลจากการศึกษารูปร่างของเซลล์ด้วยการย้อมติดสีฟลูออเรสเซนต์ การพอกพูนแร่ธาตุในกระดูก (bone mineralization) และการวิเคราะห์การแสดงออกของยีนที่เกี่ยวข้องกับการเกิดกระดูกผ่านปฏิกิริยาลูกโซ่พอลิเมอเรสเชิงปริมาณ (qPCR) พบว่า pOPN ที่ตรึงลงบนบีซีเมมเบรนซึ่งกราฟต์ด้วย PAA แสดงศักยภาพในการนำไปประยุกต์ทางวิศวกรรมเนื้อเยื่อกระดูก

สาขาวิชา ปิโตรเคมีและวิทยาศาสตร์พอลิเมอร์ ลายมือชื่อนิสิต .....

ปีการศึกษา 2559 ลายมือชื่อ อ.ที่ปรึกษาหลัก .....

ลายมือชื่อ อ.ที่ปรึกษาร่วม .....

5771989423 : MAJOR PETROCHEMISTRY AND POLYMER SCIENCE
KEYWORDS: BACTERIAL CELLULOSE (BC) / PLANT-DERIVED OSTEOPONTIN (POPN) / POLY(ACRYLIC ACID) (PAA) / BONE TISSUE REGENERATION

NICHAPA KLINTHOOPTHAMRONG: IMMOBILIZATION OF PLANT-DERIVED OSTEOPONTIN ON BACTERIAL CELLULOSE MEMBRANE FOR BONE TISSUE REGENERATION. ADVISOR: ASSOC. PROF. VORAVEE HOVEN, Ph.D., CO-ADVISOR: PROF. PRASIT PAVASANT, Ph.D., 39 pp.

Bacterial cellulose (BC) membrane is recognized as a potential material to be developed into Guided Tissue Regeneration (GTR) membrane due to its sufficient mechanical strength, biocompatibility, and ease for surface functionalization. Here in this research, plant-produced osteopontin (pOPN) was selected to be immobilized on BC surface in order to promote cell adhesion and osteogenic differentiation. BC membrane was first grafted with poly(acrylic acid) (PAA) brushes via surface-initiated reversible addition fragmentation chain transfer (RAFT) polymerization. pOPN was subsequently immobilized on the PAA-grafted BC via amidation reaction between carboxyl groups of PAA and amino groups of pOPN. ATR-FTIR and XPS analysis were used to verify the success of stepwise modification. Surface morphology of the modified BC was evaluated by FE-SEM and AFM techniques. pOPN immobilized on the BC membrane was quantified by ELISA assay. Biological functions of the pOPN immobilized PAA-grafted BC membrane (pOPN-BC) were tested against human mesenchymal stem cells (hMSCs) in comparison with commercial available recombinant OPN from mammalian cells (rOPN). Results from immunofluorescent staining assay, mineralization assay and quantitative real-time polymerase chain reaction (qPCR) subsequently suggested the potential of pOPN-BC to promote bone tissue regeneration.

Field of Study:	Petrochemistry and Polymer Science	Student's Signature .....
		Advisor's Signature .....
Academic Year:	2016	Co-Advisor's Signature .....

ACKNOWLEDGEMENTS

First of all, I would like to thank and express my deepest gratitude to my thesis advisor, Assoc. Prof. Dr. Voravee P. Hoven for her valuable advice, constructive criticism, encouragement and kindly support throughout my Master's degree program.

Moreover, I owe a deep sense of appreciation to my co-advisor, Prof. Dr. Prasit Pavasant, from Department of Anatomy, Faculty of Dentistry, Chulalongkorn University for the collaboration, valuable guidance, and kindly support for my entire research.

I wish to thank my thesis committee: Prof. Dr. Pattarapan Prasassarakich, Asst. Prof. Dr. Varawut Tangpasuthadol, and Asst. Prof. Dr. Punnama Siriphannon for giving their valuable time to review my thesis and give the important suggestion for my work.

For Program in Petrochemistry and Polymer Science, I would like to thank all lecturers who provided me the fundamentally knowledge that is important for the developing process in my work.

Special thanks are extended to Miss Daneeya Chaikiawkeaw, from Department of Anatomy, Faculty of Dentistry, Chulalongkorn University for assistance and suggestion in cells studies, her kindly help and co-operation.

This research was performed at Oraganic Synthesis Research Unit (OSRU), Department of Chemistry, Faculty of Science, Chulalongkorn University and the financial support was provided by Thailand Research Fund RSA5980071 and IRN59W0001. NK acknowledges the Science Achievement Scholarship of Thailand (SAST) for a M.Sc. scholarship.

Furthermore, l am extremely thankful to all of VH research group members in Oraganic Synthesis Research Unit (OSRU) for their friendship and endless help during my thesis work.

CONTENTS

Page

Page

LIST OF FIGURES

Figures Pages

LIST OF TABLES

Table Pages

LIST OF ABBREVIATION

AA	: Acrylic acid
ACVA	: 4,4′-Azobis(4-cyanovaleric acid)
AFM	: Atomic-force microscopy
ALP	: Alkaline phosphatase
ARS	: Alizaline Red S staining
ATR-FTIR	: Attenuated total reflection-Fourier transform infrared spectroscopy
BC	: Bacterial cellulose membrane
COL1	: Collagen type 1
CPC	: Cetyl-pyridinium choride
CPD	: 4-Cyano-4-(thiobenzoylthio)pentanoic acid
DCC	: Dicyclohexylcarbodiimide
DMAP	: 4-Dimethylaminopyridine
DMF	: Dimethylformamide anhydrous
DP	: Degree of polymerization
cDNA	: Complementary deoxyribonucleic acid
EDC	: 1-Ethyl-3-(3-dimethylaminopropyl)carbodiimide
ELISA	: Enzyme-Linked Immunosorbent Assay
FDA	: Food and Drug Administration
FE-SEM	: Field emission-scanning electron microscope
FTIR	: Fourier-Transform Infrared Spectroscopy

GAPDH	: Glyceraldehyde-3-phosphate dehydrogenase
GTR	: Guided Tissue Regeneration
hMSCs	: human mesenchymal stem cells
^{1}H-NMR	: Proton nuclear magnetic resonance
hPDLs	: human periodontal ligament stem cells
ITG1	: Integrin-beta1
MTT	: (4,5-dimethylthiazol-2-yl)-2,5-diphenyltetrazolium bromide
NHS	: N-hydroxysuccinimide
PBS	: Phosphate buffered saline
pOPN	: Plant-produced Osteopontin
pOPN-BC	: Plant-produced Osteopontin immobilized pol(yacrylic acid) grafted bacterial cellulose membrane
PAA	: Poly(acrylic acid)
RAFT	: Reversible addition-fragmentation chain transfer
RNA	: Ribonucleic acid
rOPN	: recombinant OPN from mammalian cell (HEK-293)
rOPN-BC	: recombinant OPN from mammalian cell (HEK-293) immobilized pol(yacrylic acid)-grafted bacterial cellulose membrane
RUNX2	: Runt-related protein-2
XPS	: X-ray photoelectron spectroscopy
qPCR	: Quantitative real-time polymerase chain reaction

CHAPTER I
INTRODUCTION

1.1 Introduction

Bone defects resulted from trauma, surgery, periodontal disease or infection remains a major health problem. Various methods have been developed for bone regeneration such as transplantation from patient (autograft), from another human (allograft) and from another species (xenograft). However, limitation of tissue donor quality and quantity in autograft and the risk of graft rejection and pathogen transmission in allograft and xenograft require the critical consideration. [1, 2] Guided Tissue Regeneration (GTR) membrane is reported as one of the commonly used barrier to induce regeneration by isolating the bone defect from the surrounding soft tissue such as gum tissue and providing spaces for new bone formation.

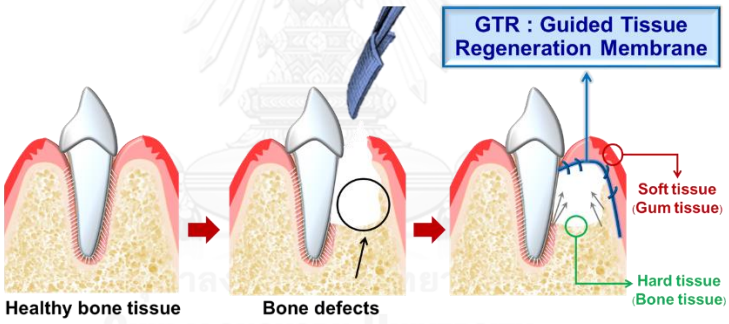

Figure 1.1 A schematic represents GTR membrane to induce regeneration by providing spaces for new bone growth.

GTR membrane can be categorized into 2 types. [3, 4] 1) Resorbable membrane such as degradable collagen and poly(lactic-co-glycolic acid) (PLGA) show excellent bone healing and tissue-integration without requiring for surgical removal. [5] However, it is difficult to predict the rate of membrane resorption and to examine the regenerated bone tissue in clinical settings. 2) Non-resorbable membrane including titanium mesh and expanded polytetrafluoroethylene (Teflon) are superior for space-maintaining and structural integrity during implantation. Nevertheless, cellular

adhesion is quite limited. [3, 6] Difficult surface modification of Teflon and structural rigidity of titanium somewhat limit their versatility for clinical utilization.

Bacterial cellulose membrane (BC) is a product from the primary metabolism of many bacteria such as Gluconacetobacter (formerly Acetobacter), Agrobacterium, and Rhizobium. As shown in **Figure 1.2**, cellulose biosynthesis is a multi-step reaction involving individual enzymes, catalytic complexes and regulatory proteins. Although the biosynthesis process is complicate and not clearly understood, there are four key steps for metabolizing glucose to pure BC. First of all, the phosphorylation of glucose by glucokinase take place, follow by the isomerization of glucose-6-phosphate (Glc-6-P) to glucose-1-phosphate (Glc-1-P) by phosphoglucomutase. Thirdly, uridine diphosphoglucose (UDPGlc) is synthesized by UDPGlc-phyrophosphorylase (UGPase). Finally, the glucose is polymerized into a β-1,4 glucan chain to create the ribbon-like structure of cellulose. After synthesized inside the bacteria, the fibril is continuously extruded between the outer and cytoplasm membranes to from BC. Moreover, the prior report speculated that BC is formed due to a self-defense mechanism of bacteria to protect itself from the UV damaging effects, or to secure itself with sufficient oxygen supply by floating at the air-liquid interface. [7]

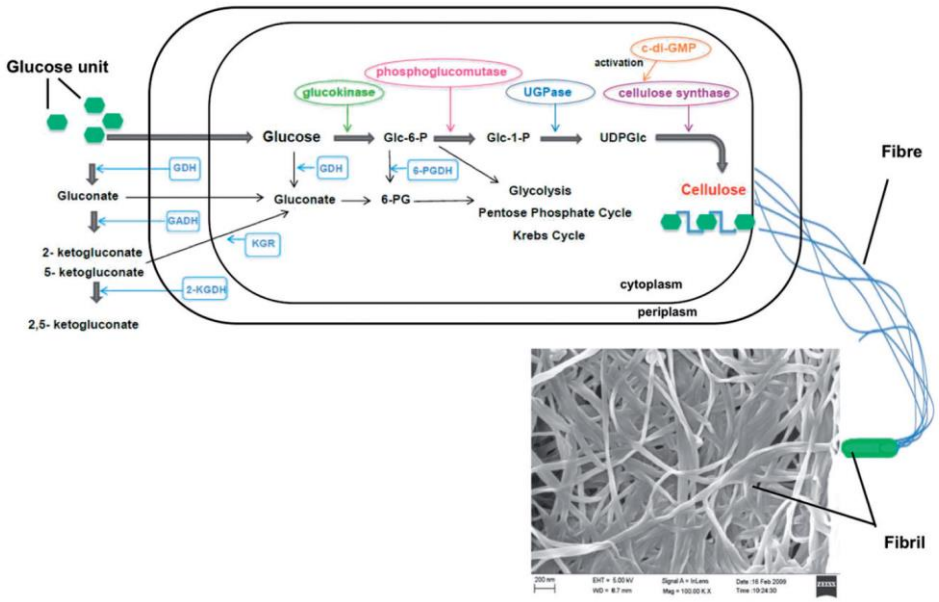

Figure 1.2 A schematic performing the metabolic pathways of bacteria (A. xylinum) and the assembly of cellulose fiber to form BC. [7]

Furthermore, BC exhibits unique properties including high water content and high degree of crystallinity, three-dimensional nanostructure which mimics the conformation of the extracellular-matrix, high purity without the hemicellulose and lignin contamination, and its simple production that allows BC to be more attractive than cellulose from plant. Owing to its superior mechanical property and ease of process, different BC shape (such as membrane, pellets or thin fibrous), BC have been approved by Food and Drug Administration (FDA) for wound dressing, cartilage repairing, and widely used for tissue engineering application. [8-10] The examples of BC applied for various applications are shown in **Figure 1.3**.: (a) BC vascular tubes with different dimensions, (b) Vascular prostheses made of CNF-polyurethane placed between the brachiocephalic trunk and the right common carotid artery in patient, (c) pig meniscus (left) compared with BC hydrogel (right), (d) silicone mold to reproduce the outer ear (left) and 3D BC implant prototype produced in the shape of the whole outer ear using the 3T MRI scanning technique (right). [11]

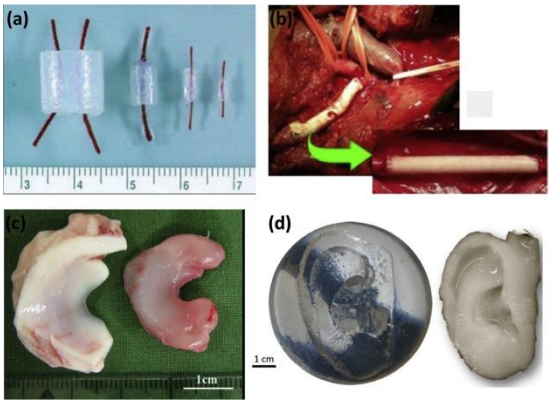

Figure 1.3 Various BC applied as the biomaterials: (a) BC tubes, (b) Vascular prostheses made of CNF-polyurethane ,(c) pig meniscus (left) and mimic BC hydrogel (right), (d) silicone mold (left) and 3D BC implant prototype of outer ear (right) [11]

In addition, BC is recognized as a potential non-resorbable GTR barrier due to its sufficient tensile strength, elastic modulus, porosity, and ease for functionalization via multiple hydroxyl groups available on its surface. Although BC did not induce inflammatory response, the differentiation and proliferation rate of cells cultured on BC was lower than those of cells cultured on collagen membrane. [12, 13] Consequently, several studies have aimed to improve BC with even greater biological responses such as providing structural motifs [1, 14] and modification of surface materials with physical and chemical reaction such as plasmas [9] which are described afterward.

In 2015, Kirdponpattara *et al.* [14] fabricated highly interconnected pores bacterial cellulose–alginate composite (N-BCA) by freeze drying and crosslinking with Ca^{2+} to maintain its stability. They found that N-BCA promoted adhesion and proliferation of human gingival fibroblast (GF) on the modified surface as compared with those of the single-component scaffolds.

In 2012, Kurniawan *et al.* [9] modified BC with oxygen (BC-O2), nitrogen (BC-N2), and tetrafluoromethane (BC-CF4) plasmas in order to enhance cell affinity with highly hydrophilic surface. They found that BC-CF4 exhibited superior impacts on promoting the Chinese hamster ovary cell lines (CHO) adhesion and proliferation as compared

with those on the pure BC, BC-O2, and BC-N2 having different functional groups on their surfaces after the treatment with different plasma.

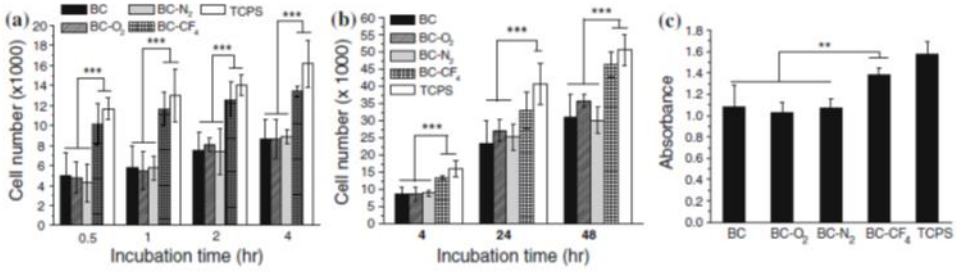

Figure 1.4 CHO cell attachment on BC, BC-O2, BC-N2 and BC-CF4 cultivated with different time interval for (a) 0.5–8 h, (b) 4–48 h, (c) CHO cell viability by MTT assay after 48 h of culture. [9]

Most of studies focus on the combination of the materials with bioactive molecules such as hydroxyapatite [15], gelatin [16], hyaluronic acid (HA) [17], collagen peptide [18, 19], and bone morphogenic proteins (BMPs) [20] that specifically bind to cell surface receptor and assume some specific pattern of gene expression leading to tissue regeneration.

Osteopontin (OPN) is an extracellular glycosylated phosphoprotein [21] found abundantly in the mineral/tissue interface of bone and has molecular weight ranging from 41 to 75 kDa due to the difference on degree of phosphorylation after post-translation modifications. [22] Because different cellular sources of OPN might have diverse structural characteristics [23], OPN is involved in various biological functions among the variety of cell lineages. [24, 25] Moreover, OPN plays a crucial role in cell adhesion [21, 26], bone formation [27], wound healing [28], as a result of its containing significant amino sequences, RGD and SVVYGLR that mainly interact with various α_v (particularly $\alpha_v\beta_1$, $\alpha_v\beta_3$, $\alpha_v\beta_5$) and $\alpha_9\beta_1$, $\alpha_4\beta_1$, $\alpha_4\beta_7$ integrin receptors at the cell's surface, respectively. [22, 23]

There were some studies that evaluated cellular response of osteopontin (OPN) to enhance bone tissue regeneration such as in 2003, Martin *et al*. [21] covalently immobilized rat OPN onto poly(2-hydroxyethyl methacrylate) [poly(HEMA)] using 1,1

carbonyldiimidazole (CDI) as a coupling agent. They found that OPN immobilized poly(HEMA) supported adhesion of endothelial cells even greater than those of the control as shown in **Figure 5**. (right),.

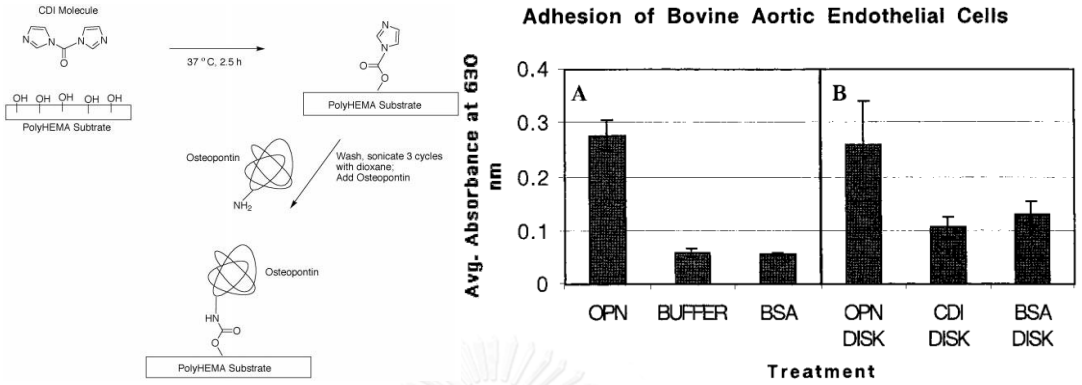

Figure 1.5 Schematic diagram of the poly(HEMA) immobilized with OPN via CDI agent (left) and quantification of endothelial adherent cells on (A) plated OPN, buffer, and BSA, (B) OPN-immobilized poly(HEMA), BSA-immobilized poly(HEMA), and CDI-treated poly(HEMA) without OPN (right). [21]

In 2014, Kim *et al.* [26] modified a film of polycaprolactone (PCL) by grafting with 1,6-hexanediamine having amino end groups (PCL-NH_2) followed by immobilization of two cross-linked bone matrix proteins (collagen type 1 and OPN) onto the surfaces. *In vitro* studies with human adipogenic mesenchymal stem cells (hADMSC) indicated that hADMSC spreading and attachment on the modified PCL was better than those on unmodified PCL.

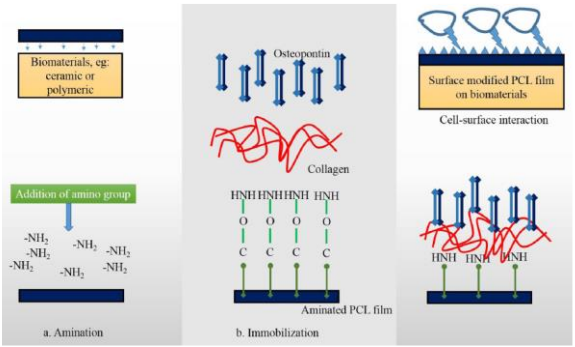

Figure 1.6 Schematic diagram showing mixed COL1-OPN proteins immobilized on the PCL film grafting 1,6-hexanediamine. [26]

In 2011, Jensen *et al*. [27] prepared the composite of hydroxyapatite (HA) nanoparticles immobilized with bovine OPN and mixed with poly-D,L-lactic-acid (PDLLA); (OPN-COMP). The functionalized composite coated on a commercially titanium implant was investigated for the osteoconductivity in a canine gap model for four weeks. The result showed that there was a significantly larger amount of newly formed bone covered the OPN-COMP surface compared with pure PDLLA/HA composite (COMP) of the inner zone 1.

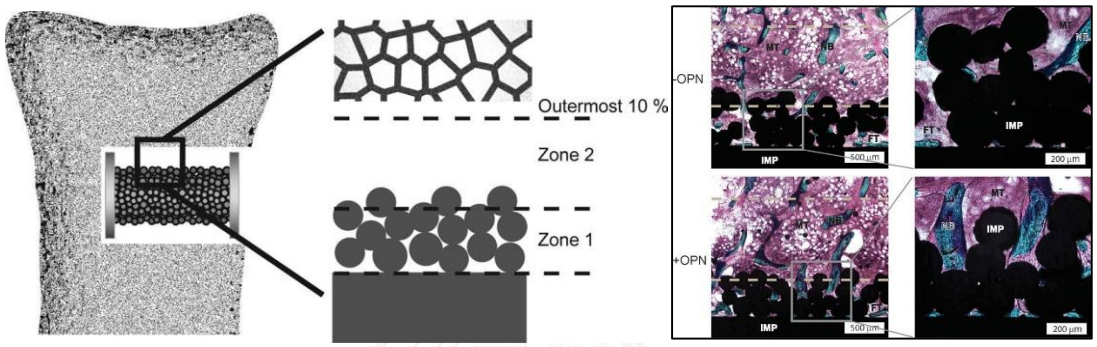

Figure 1.7 Canine implant model (left) and representative pictures of the implant surfaces coated with COMP (-OPN) and OPN-COMP (+OPN). IMP: implant, NB: new bone, FT: Fibrous tissue, MT: marrow tissue. [27]

Interestingly, most of early studies were only about the bioactivity of OPN produced from mammalian cell which is quite expensive. On the other hand, we recently have extracted recombinant OPN from tobacco (Nicotiana benthamiana) with high yield and low production cost and demonstrated that the recombinant protein could induce the expression of osteogenic related genes, suggesting the ability of the protein to induce new bone formation. [29] Therefore, we would like to examine the potential of the plant-produced osteopontin (pOPN) immobilized on BC surface to promote cell adhesion and osteogenic differentiation.

To inherit BC with even greater number of active sites for pOPN conjugation, several methodology have been reported [15, 17-20] such as in 2015, Ahn *et al.* [16] immobilized 3-aminopropylphosphoric acid (ApA) on carboxylated cellulose-nanofibrils (CNF-COOH) via carbodiimide crosslinking (EDC/NHS) in order to mimic moiety found in biological molecules towards intensification of Hydroxyapatite-like crystals deposition on the surface. Then, CNF-COOH-ApA was composited with gelatin

to possess suitable micro-structure and strength. Results from *in vitro* biological responses of mesenchymal stem cells suggested that the modified composite exhibited improved cell viability, proliferation, and mineralization for bone tissue engineering.

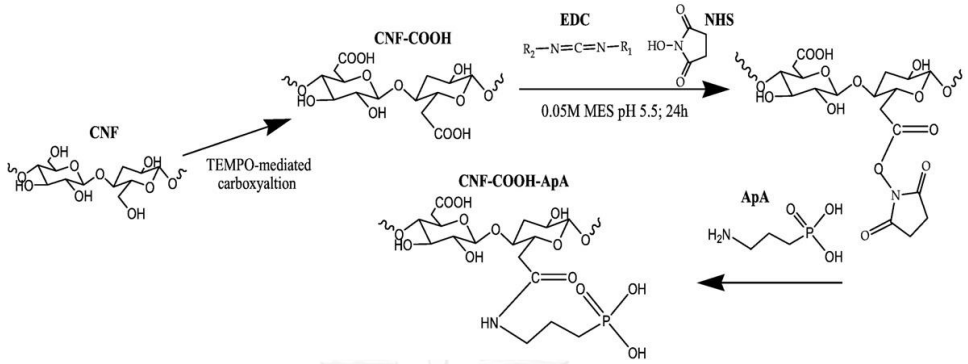

Figure 1.8 Schematic diagram of CNF-COOH modification with ApA via carbodiimide chemistry. [16]

In 2015, Wen *et al*. [18] oxidized BC into dialdehyde bacterial cellulose (DBC) by regioselective oxidation, the DBC containing aldehyde group was covalently bond to amino group of collagen peptide (Col-p) via Schiff's base reaction. Fibroblast cells cultured on the DBC/Col-p composite exhibited good cellular affinity for adhesion and proliferation.

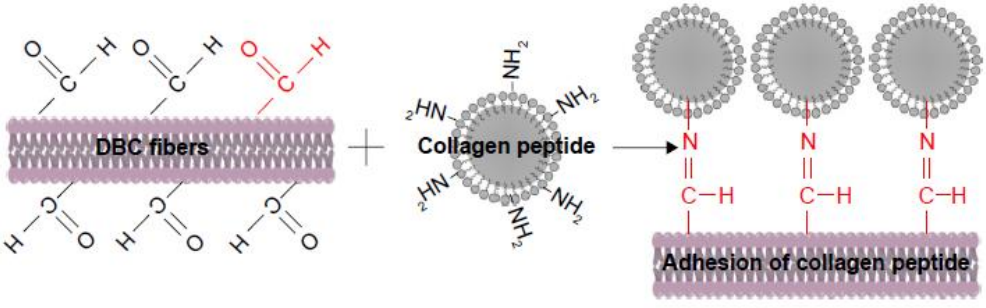

Figure 1.9 Schematic illustration of DBC/Col-p composite membranes preparation. [18]

In 2014, Cho *et al*. [20] developed a biodegradable poly(L-lactide) (PLLA) membrane immobilized with BMP-2 using polydopamine chemistry. After cultured with human mesenchymal stem cells (hMSCs), the BMP-2-modified fibers demonstrated

superior potential on cell adhesion, proliferation, and osteogenic differentiation. Additionally, a calvarial critical size defect mouse model implanted with BMP-2-modified fiber showed enhanced bone formation compared to a control sample

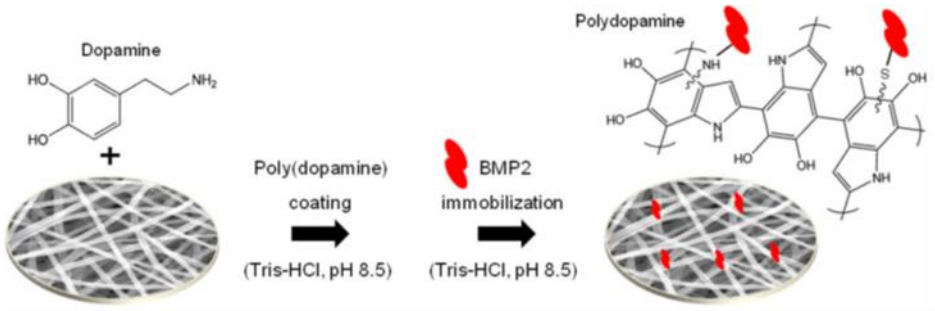

Figure 1.10 A schematic preparation of the polydopamine-coated poly(L-lactide) (PLLA) nanofibers with immobilized BMP-2. [20]

Here in this research, an approach of covalent immobilization of pOPN via polymer brushes of poly(acrylic acid) (PAA) was selected. This method offers the advantages over the physical adsorption such as providing stability of binding protein without structural denaturation and unfolding, [30, 31] and impose less effect on the bulk properties of the material. [17, 32] Owing to its rich content of carboxyl groups and high swelling in the aqueous solution, PAA provide abundant sites for protein immobilization and its binding chemistry via the EDC/NHS coupling process has been established. [30, 33-39]

In 2013, Qu *et al.* [33] reported a facile RAFT polymerization route to modified silica nanoparticles by grafting with PAA brushes (SiO_2@PAAs) as a well-controlled polymerization. Moreover, SiO_2@PAAs was immobilized with streptavidin and biotin to demonstrate the ultra-high protein immobilization capacity which is 60-fold higher than that achieved by monolayer functionalization due to abundant carboxyl groups of PAA brushes.

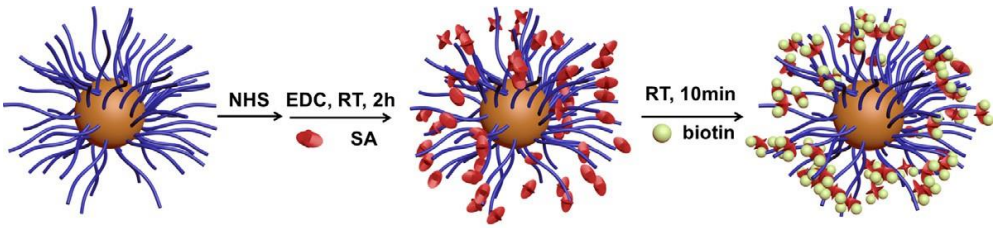

Figure 1.11 Schematic illustration of SiO_2@PAAs immobilized with streptavidin (SA) and the binding of biotin to SA. [33]

In 2014, Qu *et al.* [34] further demonstrated the superior protein (BSA) binding capacity of silica nanoparticles grafted with PAA brushes (3D SPAABs) over the conventional carboxylated SiO_2 particles (2D SiO_2–COOH). Additionally, due to the dominant desorption of BSA after physical adsorption to SPAABs, covalent bonding via EDC/NHS process provides greater effective, simple, and stable for protein immobilization though PAA brushes.

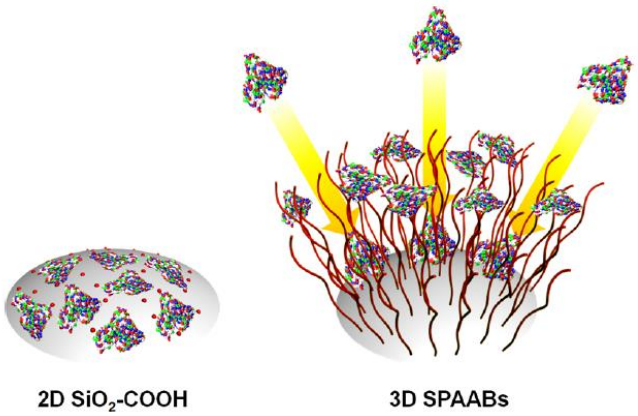

Figure 1.12 Schematic illustration of the superior capacity of the 3D SPAABs in protein immobilization compared with 2D SiO_2–COOH. [34]

In 2013, Wang *et al.* [37] fabricate 3D patterned PAA brushes on cystemine mediated gold-coated chip using microcontact printing (μCP). Additionally, to measure the specific binding of Hepatitis-B-Virus surface antibody (HBsAb), 3D PAA pattern was immobilized with the antigen (HBsAg) and BSA (blocking agent) along SPR process. They found that the 3D PAA pattern exhibits 18.3 fold higher protein loading and lower non-specific adsorption as compared with the PAA brushes-containing surface without

patterning and 2D bare gold surface, suggesting its potential be used as a clinical diagnosis by assaying of HBsAb with HBsAg concentration array chip.

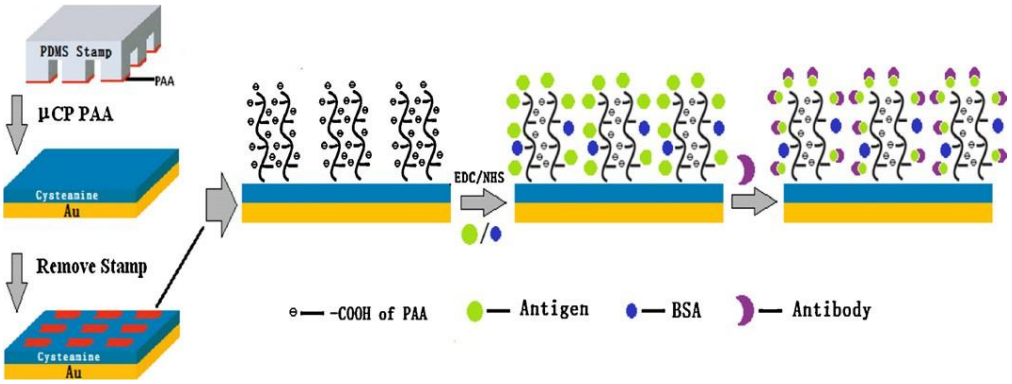

Figure 1.13 Schematic diagram of patterned PAA brushes and immunoassay along SPR process [37]

Recently, our research group [36] fabricated patterned PAA brushes containing gold nanoparticles for peptide detection. The PAA brushes was successfully generated from patterned Si-NH_2/$O(CH_2)_2(CF_2)_5CF_3$ via surface-initiated reversible addition fragmentation chain transfer (RAFT) polymerization. [40, 41] By controlling concentration of initiator versus chain transfer agent (CTA), well-controlled molecular weight with different degree of polymerization of PAA can be achieved. The general mechanism for RAFT polymerization is shown in **Figure 1.14**.

Herein this research, PAA was first grafted on BC membrane via RAFT polymerization. pOPN was subsequently immobilized on the PAA-grafted BC membrane via amidation reaction between carboxyl groups of PAA and amino groups of pOPN. The success of stepwise modification was verified by attenuated total reflection-Fourier transform infrared spectroscopy (ATR-FTIR) and x-ray photoelectron spectroscopy (XPS). To evaluate the effect of PAA grafting and pOPN immobilization, mechanical testing, field emission-scanning electron microscope (FE-SEM), and atomic-force microscopy (AFM) were conducted. ELISA was performed to quantify the amount of immobilized pOPN.

Human mesencymal stem cells (hMSCs) or human periodontal ligament stem cells (hPDLs) with its ability to differentiate into osteoblast (bone) *in vitro*, was

collected from adult teeth [42] and have been approved its stem cell properties as described previously [43]. Therefore, to evaluate the effect of pOPN for promoting cell adhesion and osteogenic differentiation, hPDLs was selected to be cultured on PAA-grafted BC immobilized with pOPN (pOPN-BC). Biological responses were evaluated by immunofluorescent staining assay, mineralization assay, and quantitative real-time polymerase chain reaction (qPCR) in comparison with the unmodified BC membrane (negative control) and PAA-grafted BC membrane immobilized with commercial recombinant OPN from mammalian cell (HEK-293) (rOPN; positive control).

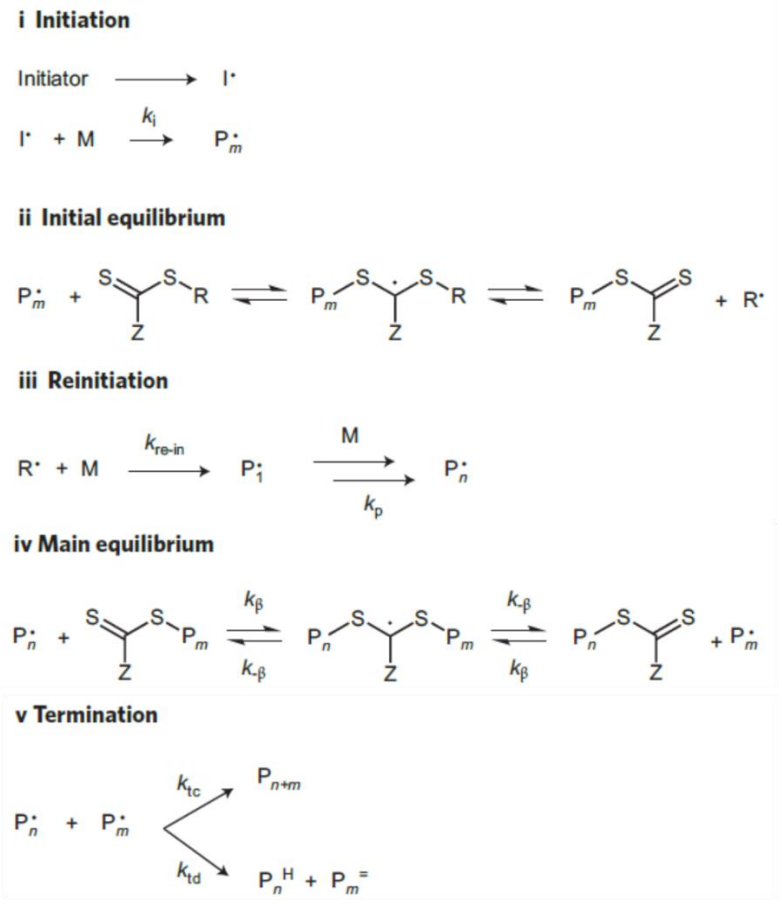

Figure 1.14 Schematic diagram of proposed RAFT Mechanism [41]

1.2 Objective

1. To prepare and characterize poly(acrylic acid) brushes-grafted BC membrane and immobilized with plant-derived OPN.

2. To determine biological functions of plant-derived OPN immobilized on poly(acrylic acid) brushes-grafted BC membrane against human mesenchymal stem cells (hMSCs).

1.3 Scope of investigation

1. Preparation and characterization of poly(acrylic acid) brushes-grafted BC membrane (PAA-grafted BC) via surface-initiated RAFT polymerization

2. Immobilization of plant-derived OPN (pOPN) on the PAA-grafted BC membrane via carbodiimide coupling

3. Characterization of surface-modified BC membranes using ATR-FTIR spectroscopy and XPS analysis

4. Investigation of surface morphology of surface-modified BC membranes by FE-SEM and AFM analysis

5. Quantification of immobilized pOPN per surface area and immobilization efficiency by ELISA assay

6. Morphological evaluation of human periodontal ligament stem cells (hPDLs) cultured on the PAA-grafted BC immobilized with pOPN using immunofluorescent staining assay

7. Determination of viability of hPDLs cultured on PAA-grafted BC immobilized with pOPN using MTT assay

Determination of bone minerialization of hPDLs cultured on PAA-grafted BC immobilized with pOPN.

8. Determination of gene expression related with osteogenic differentiation of hPDLs cultured on PAA-grafted BC immobilized with pOPN by real time-quantitative polymerase chain reaction (qPCR).

CHAPTER II
EXPERIMENTAL

2.1 Materials

Bacterial cellulose (BC) membrane was purchased from Thai-nanocellulose Ltd, Phatthalung, Thailand. Plant-derived Osteopontin (pOPN) was extracted from Nicotiana benthamiana leaves (tobacco plant) using geminiviral vector and purified by Ni affinity chromatography as described previously. [27] Recombinant osteopontin human (rOPN) expressed in HEK-293 cells from Sigma-Aldrich, USA (containing 298 amino acids, apparent molecular weight of 60.0-65.0 kDa). 4,4′-Azobis(4-cyanovaleric acid) (ACVC), 4-cyanopentanoic acid dithiobenzoate (CPD), dicyclohexylcarbodiimide (DCC), 4-dimethylaminopyridine (DMAP), and phosphate buffered saline (PBS, pH 7.4) were purchased from Sigma-Aldrich, USA. Acrylic acid (AA) and N-hydroxysuccinimide (NHS) were purchased from Aldrich, USA. 1-(3-Dimethylaminopropyl)-3-ethylcarbodiimide hydrochloride (EDC) was purchased from TCI, Japan. Dimethylformamide anhydrous (DMF) was purchased from RCI labscan, Thailand. Milli-Q water was purified by Millipore Milli-Q system; reverse osmosis, ion exchange, and filtration steps. All reagents and materials are analytical grade and used without further purification. The exception was extended to AA that was purified by vacuum distillation before used.

2.2 Characterization

^{1}H-NMR spectrum of PAA produced in solution was acquired in D_2O on a Varian, model Mercury-400 nuclear magnetic resonance spectrometer [5] operating at 400 MHz. Field Emission Scanning Electron microscope (FE-SEM) images were observed using a model JSM-7610F (Japan). Freeze-dried sample were deposited on brass stubs with a conductive carbon layer and coated with Platinum. Mechanical properties of the BC membranes after 5 min soaking in water were examined by Universal testing machine (Shimadzu, Japan) with a 500 N load cell at speed of 0.1 mm/min. The samples (n=6) were cut into 15 x 50 mm^2 for ultimate tensile stress and Young's modulus test. Compressive strength were measured on wet samples (n=10) with 15 mm diameter and 0.2 mm thickness which measured by a micrometer. The stepwise

modification BC membranes were verified by ATR-FTIR analysis that was performed at a resolution of 4 cm^{-1} and 128 scans using model Impact 410 (Nicolet, USA), in a frequency range of 400-4000 cm^{-1} using TGS detector. Atomic compositions of BC membranes were determined by x-ray photoelectron spectrometer (XPS; AXIS ULTRADLD, UK.) The base pressure in the XPS analysis chamber was about 5×10^{-9} torr. The samples were excited with x-ray hybrid mode 700x300 μm spot area with a monochromatic Al Kα 1,2 radiation at 1.4 keV. X-ray anode was run at 15 kV, 10 mA, 150 W. The photoelectrons were detected with a hemispherical analyzer positioned at an angle of 90° with respect to the normal to the sample surface. Surface roughness and morphology of the BC membranes were evaluated by Atomic-force microscopy (AFM) using Scanning Probe Microscope model NanoScope IV (Veeco, USA). Measurements were performed in air using tapping mode. Silicon-SPM-sensor with rotated tip (180°) with a resonance frequency of 204-497 kHz and a force constant 10-130 N/m were used.

2.3 Preparation of OPN immobilized PAA-grafted BC membrane

Briefly, the initiator, ACVA (0.05 M), DCC (0.05 M) and DMAP (5.00 mM) were dissolved in 20 mL DMF and continued purging with nitrogen gas for 4-6 h. The solution was transferred to freeze-dried BC membrane in a vial before being stirred at room temperature for 20-24 h. (**Step I; Figure 2.1**). Then, the BC membrane was taken out of the vial and rinsed with DMF and ethanol. The obtained initiator-grafted BC membrane was then placed in a vial containing AA (1.00 M), ACVA (2.50 mM), and CPD (0.01 M) in Milli-Q water. The surface-initiated RAFT polymerization of AA was allowed to proceed at 70 °C under nitrogen atmosphere for 20 h (**Step II; Figure 2.1**). The resulting PAA grafted-BC membrane was rinsed with ethanol and DI water then dried under vacuum. Plant-derived Osteopontin (pOPN) and recombinant OPN from HEK-293 (rOPN) were consequently immobilized on the PAA-grafted BC via amine coupling reaction. The PAA-grafted BC was cut into 24 wells-plate size and immersed in aqueous solution of 0.2 M EDC and 0.05 M NHS for 30 min. The substrate was consequently immersed in OPN solution (30 ng/mL in PBS buffer (pH 7.4)) at room temperature for 20-24 h under mild shaking (240 rpm). After rinsed with PBS and DI water, OPN-immobilized PAA-grafted BC membrane was obtained (**Step III; Figure 2.1**).

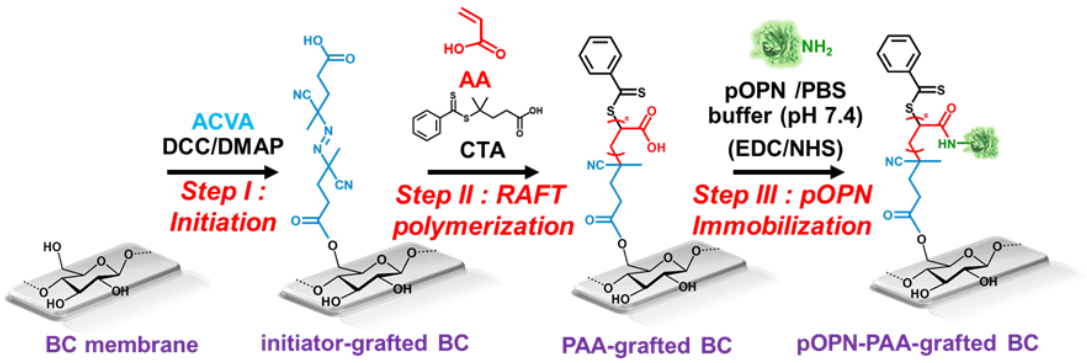

Figure 2.1. Preparation of OPN immobilized PAA-grafted BC membrane.

2.4 Enzyme-Linked Immunosorbent Assay (ELISA)

ELISA was performed to determine the amount of pOPN immobilized on the PAA-grafted BC (24 wells-plate size) by detecting the remaining pOPN in solution after the immobilization. Briefly, the pOPN solution after the immobilization step together with the solution obtained after sample washing were collected to be freeze-dried before diluting with ELISA eluent. The amount of pOPN was quantified by sandwich ELISA development kit (Sigma-Aldrich, USA). The absorbance of ELISA reaction product was measured at 450 nm, using a microplate reader (Bio Tek, ELx800, Winooski, VT, USA). The amount of remained pOPN was subtracted from the initial pOPN before surface immobilization to obtain the total pOPN that was bound to PAA-grafted BC membrane. The range of pOPN adhered on the membrane (ng/cm^2) was evaluated by compared with the surface area of modified BC (at 24 wells-plate size) which can be calculated as single-sided membrane (1.9 cm^2) or both-sided membrane (3.8 cm^2) .

2.5 Culture of human periodontal ligament cells (hPDLs)

Human mesencymal stem cells (hMSCs) are adult stem cells with its ability to differentiate *in vitro* into adipocyte, chondrocyte (cartilage), and osteoblast (bone). hMSCs was isolated from various tissue sources such as bone marrow, placenta, and dental pulp. [44] Each dental MSC population is named according to its tissue of origin, e.g. stem cells from human exfoliated deciduous teeth (SHED) and human periodontal ligament stem cells (PDLSCs or hPDLs) [42] hPDLs was collected from adult teeth which

have been approved by the Ethical Committee, Faculty of Dentistry, Chulalongkorn University (Bangkok, Thailand) and stem cell properties of hPDL cells was examined as described previously. [43] hPDLs were cultured as a monolayer in Dulbecco's modified Eagle's medium (DMEM; Gibco BRL) supplemented with 10% fetal bovine serum, 1% L-glutamine and 1% antibiotic/antimycotic (Gibco BRL). The cultures were maintained at 37 °C with 5% CO_2 in 60 mm culture dish until 100% confluent was reached. For the experiments, hPDL cells were detached by 0.25% Trypsin-EDTA (Gibco BRL) and seeded onto BC membrane seated in 24 wells plate. The BC membranes were sterilized with 70% ethanol for 15 minutes and washed twice with sterile PBS buffer before cells seeding.

2.6 Cytocompatibility Evaluation by MTT Assay

The MTT (3-(4,5-dimethylthiazol-2-yl)-2,5-diphenyltetrazolium bromide) tetrazolium reduction assay was used to evaluate cell viability of hPDLs after being cultured for 24 h. hPDLs were plated on different BC membranes, at initial density of 50,000 cells/well as a monolayer in Hyclone Minimum Essential Medium (MEM) with Earle's Balanced Salts (MEM/EBSS; GE healthcare, Logan, Utah, USA) supplemented with 10% fetal bovine serum, 1% L-glutamine, and subsequently maintained under 5% CO_2 at 37 °C. After 24 h, the media was removed, 0.5 mg/mL of MTT solution without phenol red (Sigma, USA) was added and incubated for 15 min at 37 °C. The reaction mixture was removed and the purple formazan crystals was subsequently eluted by 1 mL of glycine buffer: DMSO (1: 9) solution. The quantity of formazan which to presumably proportional to the amount of viable cells was measured by recording changes in optical density (OD) at 570 nm using a microplate reader following **Equation 2.1**. OD control and OD sample is defined as optical density of the unmodified BC and the modifed BC membrane, respectively.

Determination of % cell viability from MTT assay

$$\%\textbf{cell viability} = \left\{\frac{OD_{sample}}{OD_{control}}\right\} \boldsymbol{x}\ \mathbf{100} \qquad (2.1)$$

2.7 Immunofluorescent Staining Assay

Morphology of hPDLs cultured on BC membranes was investigated by Immunofluorescent staining. After being cultured on different BC membranes for 24 h, hPDLs were fixed with 4% (v/v) formaldehyde in PBS buffer (pH=7.4) for 30 min. The cell-cultured membranes were treated with 0.1% (v/v) TritonX-100 and 1% BSA in PBS buffer (pH 7.4) to reduce non-specific background for 5 and 30 min, respectively. The actin filaments were counter-stained with Phalliodin-Rhodamine dye (1:200, Thermo Fisher Scientific, USA) for 20 min followed by nuclei staining with DAPI (1:5000, Sigma-Aldrich, USA) for 20 min. The cell-cultured membranes were rinsed twice with PBS buffer after each step. Finally, the cell morphology was observed under a fluorescent microscope (ZEISS Observer.Z1).

2.8 Quantitative Real-time Polymerase Chain Reaction (qPCR).

To further confirm the efficacy of pOPN for tissue regeneration, several specific makers associated with osteogenic differentiation were evaluated by qPCR. First, hPDLs were cultured on BC membranes at 80,000 cells/well under non-osteogenic medium condition for 1 and 3 days. Total RNA was consequently extracted from the cultured cells with Trizol reagent (Molecular Research Center, Cincinnati, OH) and quantified by measuring the absorbance at 260 nm using a spectrophotometer (NanoDrop 2000, Thermo Scientific, USA). One nanogram of total RNA per sample was conversed into complementary DNA (cDNA) with Reverse transcriptase enzyme (RT) (Promega, Madison, WI, USA). qPCR reaction was conducted by a LightCycler instrument (Roche Diagnostics, USA) with the LightCycler 480SYBR Green-I Master Kit according to the manufacturer's recommendations. The expression of osteogenic marker was quantified by RelQuant software (Roche Diagnostics, USA) and normalized to the control samples (unmodified BC) with glyceraldehyde-3-phosphate dehydrogenase (GAPDH) as the internal control. The primers sequences as shown in **Table 2.1**.

Table 2.1 Primers used for quantitative real-time polymerase chain reaction (qPCR).

Primer	Forward/Reverse	Primer sequence (5'-3')
GAPDH	Forward	CAC TGC CAA CGT GTC AGT GGT G
	Reverse	GTA GCC CAG GAT GCC CTT GAG
ALP	Forward	CGA GAT ACA AGC ACT CCC ACT TC
	Reverse	CTG TTC AGC TCG TAC TGC ATG TC
COL1	Forward	CTG GCA AAG AAG GCG GCA AA
	Reverse	CTC ACC ACG ATC ACC ACT CT
ITGB1	Forward	Agg AAC AgC AgA gAA gCT CA
	Reverse	AgC CgT gTA ACA TTC CTC CA
RUNX2	Forward	ATG ATG ACA CTG CCA CCT CTG A
	Reverse	GGC TGG ATA GTG CAT TCG TG

2.9 Mineralization Assay

To verify the potential of immobilized OPN in promoting osteogenic differentiation, a level of calcium deposition after 11 days of hPDLs culturing on OPN-immobilized BC membranes in osteogenic medium condition (Dulbecco's modified Eagle's medium supplemented with 50 µg/ml of ascrorbate-2-phosphate, 10 mM β-glycerophosphate and 100 nM dexamethasone) by using Alizaline Red S staining (ARS) was evaluted. The cells were fixed with cold methanol for 10 min and washed twice with PBS buffer (pH=7.4). The cell-cultured BC membranes were incubated with 2% (v/v) ARS solution (Sigma-Aldrich, USA) at room temperature for 5 min. After removal of ARS by washing twice with DI water, the stained BC membranes were observed under a digital camera. To quantify amount of calcium mineralization, ARS was destaining with 10% cetyl-pyridinium choride (CPC) (sigma) in 10 mM sodium phosphate for 30 min at room temperature. The absorbance was determined at 570 nm using a microplate reader (Bio Tek, ELx800, Winooski, VT).

2.10 Statistical Analysis

Statistical analysis was performed using SPSS version 16.0 software. The difference between measurements of the mechanical properties and the cellular responses between the two samples were examined by using student's t-test and student's pair t-test, respectively. Values are expressed as the mean ± standard deviations (SD). Statistical significant was accepted for p values < 0.05.

CHAPTER III
RESULT AND DISCUSSION

3.1 Preparation and Characterization of PAA-grafted BC Membrane

PAA simultaneously formed in solution during RAFT polymerization from the "sacrificial" initiator added, was characterized by ^{1}H-NMR to determine percentage of conversion, degree of polymerization [14], and molecular weight (M_n) of PAA grafted on the surface [36]. The conversion of PAA was determined from ^{1}H NMR spectra of crude PAA before dialysis (**Figure 3.1a**) using **Equation 3.1** that can be calculated from the relative ratio between the peak integration of protons from the PAA backbone (H_c,H_d ;1.4-2.4 ppm) and methylene protons of AA monomer ($\underline{CH_2}$=CH(COOH)) (5.7-6.3 ppm.). DP and M_n was determined by ^{1}H NMR spectra of pure PAA after dialysis (**Figure 3.1b)**, from the relative ratio between the peak integration of protons from PAA backbone [H_c, H_d] and protons from the dithiobenzoate groups at the chain end of PAA [H_e, 7.2-7.9 ppm] using **Equation 3.2** and **Equation 3.3,** respectively. Moreover, the calculated M_n closely resembled to the target M_n with 90% conversion suggesting that the RAFT process was well controlled.

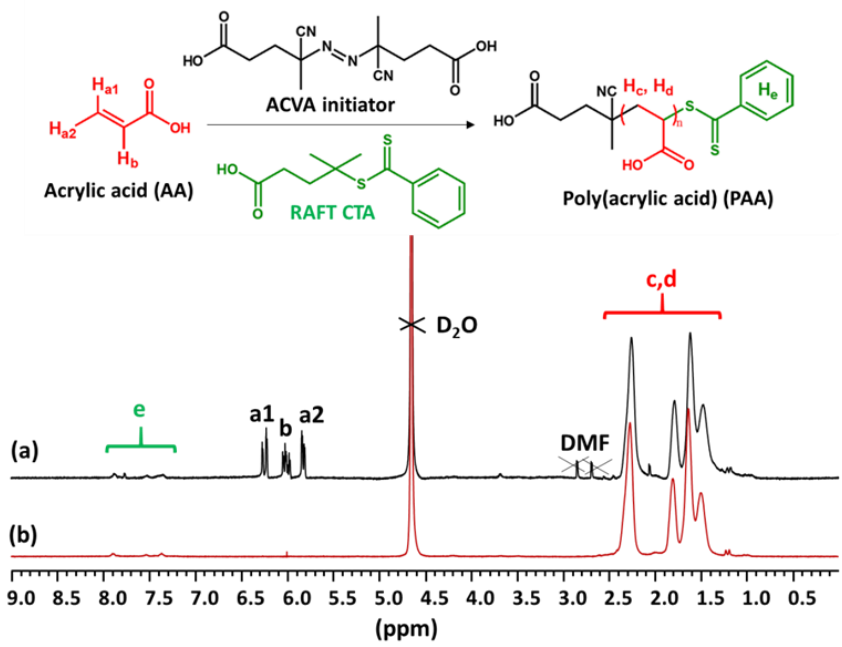

Figure 3.1. ^{1}H NMR spectrum of (a) crude PAA before dialysis in D_2O and (b) PAA after dialysis in D_2O

Determination of molecular weight of PAA from ^{1}H NMR data

$$\%\mathbf{Conversion} = \left\{\frac{\int H_{c,d},}{(\int H_{a,b}+\int H_{c,d})}\right\} \boldsymbol{x}\ \mathbf{100} \quad (3.1)$$

$$\mathbf{Degree\ of\ Polymerization\ (DP)} = \left\{\frac{\int \boldsymbol{Ha,b}}{\mathbf{3}}\right\}/\left\{\frac{\int \boldsymbol{Hc}}{\mathbf{5}}\right\} \quad (3.2)$$

$$\mathbf{M_n\ of\ PAA} = \{(72.06 \times \mathrm{DP}) + 279.38\}\ \mathbf{x}\ (\%\mathrm{conversion}) \quad (3.3)$$

Where MW (AA) = 72.06 g/mol, MW (CTA) = 279.38 g/mol]

Morphology of the BC membrane after PAA grafting was also evaluated as a function of the degree of polymerization [14] of PAA varying ratio of [AA]/[CTA] during surface-initiated RAFT polymerization. Field emission scanning electron microscope (FE-SEM) images illustrated morphology of nanofibrous BC membranes grafted with different DP of PAA brushes (**Figure 3.2**). In comparison with the unmodified BC, it is found that the porous structure of BC was preserved after PAA grafting with DP of 100 and 200, but not with 300. This data presumably suggest that the quantity of PAA can be proportionally tuned as a function of DP of PAA designated in solution.

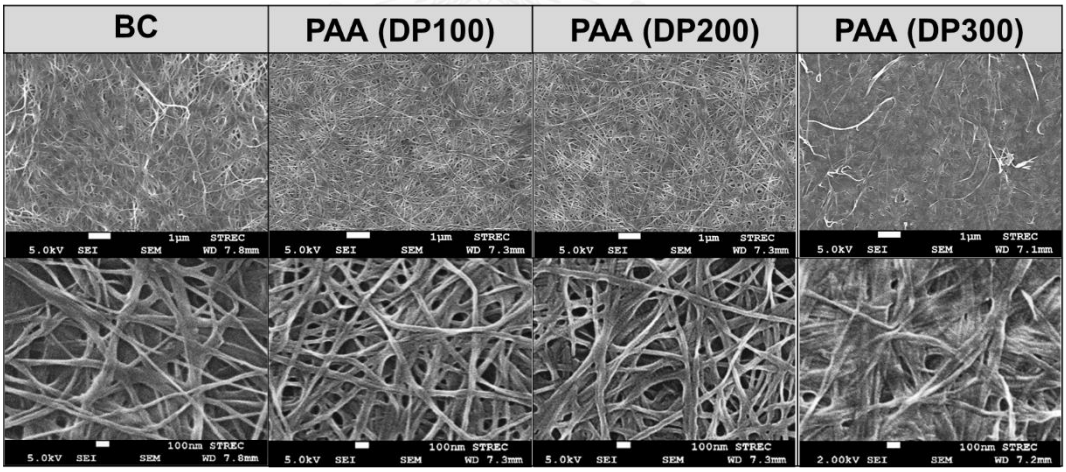

Figure 3.2. Surface morphology of unmodified BC and BC membranes grafted with PAA of different DP (100, 200, and 300) as evaluated by FE-SEM [upper row : scale bar =1 μm (5,000X); lower row : scale bar =100 nm (30,000X)].

Immobilization of OPN on the PAA-grafted BC Membrane Mechanical properties of the BC membranes in wet state in terms of ultimate tensile stress, Young's modulus,

and compressive strength are displayed in **Figure 3.3**. The ultimate tensile stress of the unmodified BC (BC) and PAA-grafted BC was 5.62 ± 2.08 and 6.70 ± 1.17 MPa respectively (n=6), and Young's modulus was 13.67 ± 5.53 and 18.17 ± 3.20 MPa respectively (n=6). The compressive strength was measured as 0.5404 ± 0.01 and 0.5429 ± 0.01 MPa respectively (n=10). No statistical significance of the difference between the two samples was observed based on 95% confidence interval. Therefore, we could confirm that such a thin layer of surface-grafted PAA imposes insignificant influence on the bulk properties especially mechanical strength of the BC membrane. In comparison with the collagen and BC membrane (tensile stress: 2.88 ± 0.33 MPa, Young's modulus: 644.71 ± 15.23 MPa) reported by others [12], ours PAA-grafted BC membrane exhibited better flexibility due to its higher tensile stress and lower Young's modulus. Additionally, its higher compressive strength over the prior BC having the same thickness (compressive strength: <0.1 MPa) [45] indicated more rigidity and strength that may be implied to the higher compact structure of our BC networks than those in the prior report.

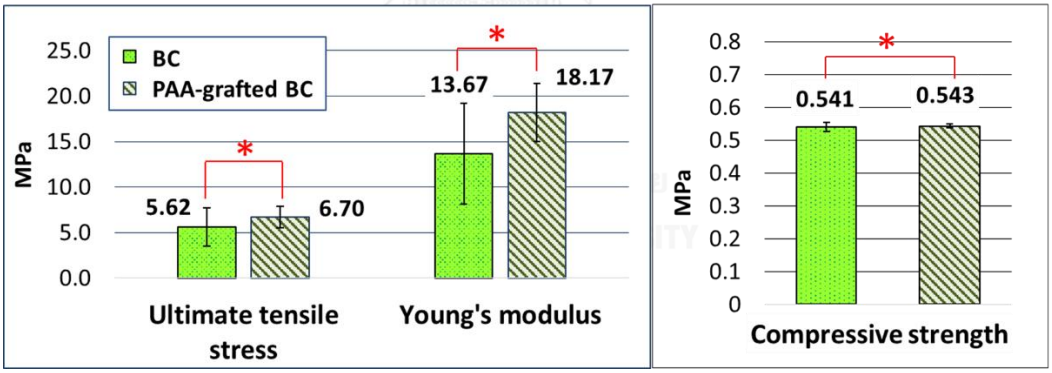

Figure 3.3 Ultimate tensile stress, Young's modulus, and compressive strength (MPa) of unmodified BC and PAA-grafted BC membrane (*$p < 0.05$).

Immobilization of OPN on the PAA-grafted BC Membrane. The success of stepwise modification could be verified by ATR-FTIR and XPS analysis. The ATR-FTIR spectra of the unmodified BC exhibited the characteristic band of cellulose (**Figure 3.4a**) at 3350 and 2900 cm^{-1}, assignable to O-H and C-H stretching, respectively. The strong C=O stretching peak at 1719 cm^{-1} appearing in the PAA-grafted BC membrane (**Figure 3.4b**) confirms the presence of PAA that grafted on the BC surface. The

absorption bands at 1643 and 1540 cm^{-1} (**Figure 3.4c**) corresponding to C=O stretching (amide I) and N-H bending (amide II), respectively, suggested that OPN have been immobilized on the BC surface bearing PAA.

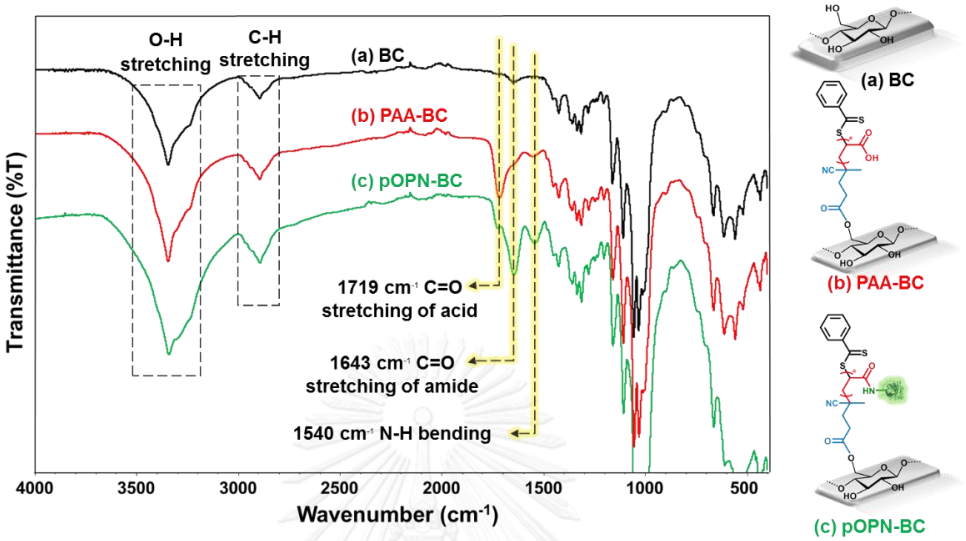

Figure 3.4 ATR-FTIR spectra of (a) unmodified BC, (b) PAA-grafted BC and, (c) pOPN immobilized PAA-grafted BC.

To further confirm the presence of PAA and OPN on the BC membrane, atomic compositions of the BC membranes was determined by x-ray photoelectron spectroscopy (XPS). XPS spectra are shown in **Figure 3.5** and atomic composition data are summarized in **Table 3.2** and **Table 3.3**. The unmodified BC consisted mostly C and O of which signal appearing at the binding energy of 285 and 532 eV, respectively. After being grafted with PAA, carbon composition was increased from 58.62% to 65.46%. Moreover, the elevating N/C atomic ratio from 1.63 of PAA-grafted BC to 3.83 of pOPN-BC verified the success of pOPN immobilization. The C1s deconvolution peaks depicted in **Figure 3.5** show 4 types of carbon: C-C/C-H (283.3 eV), C-OH/C-OC (285 eV), C=O/O-C-O (286.5 eV) and O-C=O/N-C=O (287.7 eV). The PAA-grafted BC exhibited high proportion of O-C=O peak to C-C/C-H peak over the BC as a consequence of carboxyl groups introduced from PAA. In addition, the intensity of (O=C,O-C=O)/(C-C,C-H) peak ratio of PAA-BC (**Table 3.3**) was increased after pOPN immobilization from 0.56

to 1.06 which suggested the presence of pOPN immobilized on the BC membrane enriched with oxygen-containing compound.

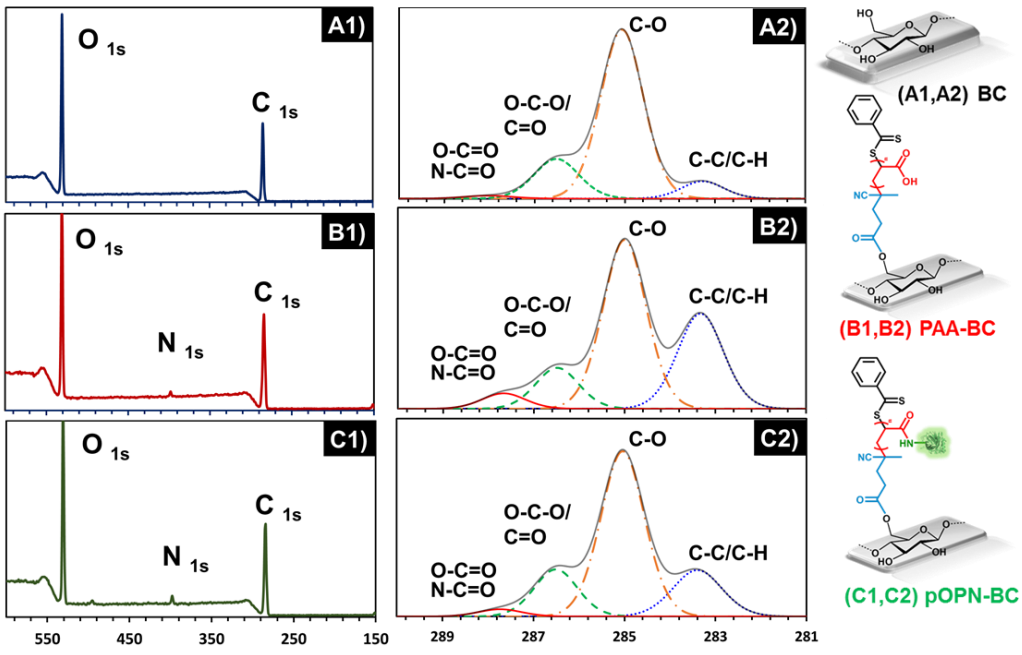

Figure 3.5 XPS wide scan spectra of BC (A1), PAA-BC (B1), pOPN-BC (C1) and deconvolution of their respective C1s peaks (A2), (B2) and (C2).

Table 3.2 Atomic composition and %N/C ratio obtained by XPS analysis for unmodified BC (BC), PAA-grafted BC (PAA-BC) and pOPN immobilized PAA-grafted BC (pOPN-BC).

Sample	Atomic Composition %				%N/C
	C	O	N	S	
BC	58.62	41.38	0.00	0.00	0.00
PAA-BC	65.46	33.39	1.07	0.08	1.63
OPN-BC	62.48	35.12	2.39	0.04	3.83

Table 3.3 C1s XPS spectra for unmodified BC (BC), PAA-grafted BC (PAA-BC) and pOPN immobilized PAA-grafted BC (pOPN-BC).

Binding type	(C-C,C-H)	(C-OH, C-O-C)	(C=O, O-C-O)	(O-C=O, N-C=O)	(C=O,O-C=O)/ (C-C,C-H)
Energy (eV)	283	285	286.5	287-288	
BC	7.6	72.9	18	1.5	2.57
PAA-BC	30.9	51.7	12.6	4.8	0.56
pOPN-BC	19.3	60.7	17.3	2.7	1.06

To evaluate the effect of the PAA grafting and pOPN immobilization on the BC surface morphology, FE-SEM and AFM analysis were performed. in FE-SEM and AFM analysis (**Figure 3.6**) revealed that the fibrous-like texture and surface roughness of the BC membrane was not altered upon PAA grafting. After OPN immobilization, accumulation of spherical-like particles on the all over nanofibrils of the BC membrane was observed suggesting the presence of OPN.

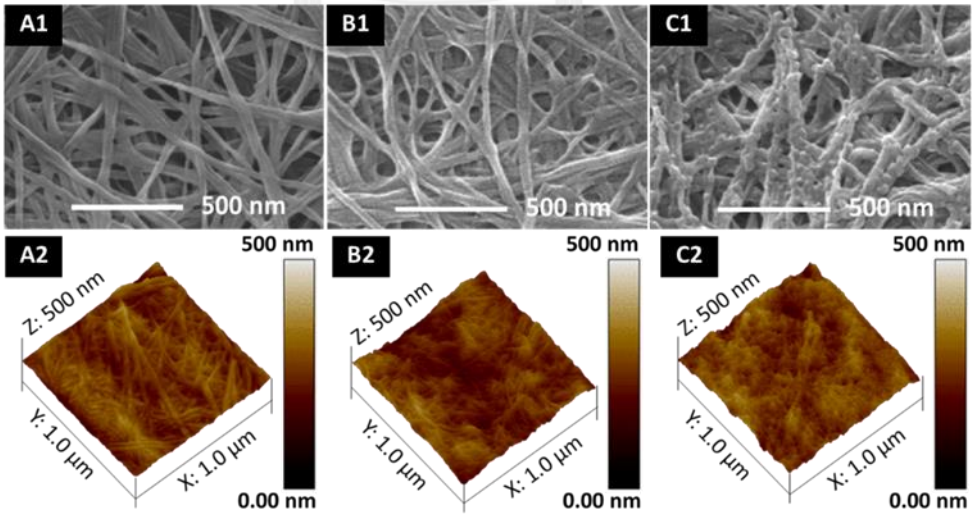

Figure 3.6 Surface morphology of unmodified BC (A1, A2), PAA grafted BC (B1, B2) and pOPN immobilized PAA-grafted BC (C1, C2) as evaluated by FE-SEM (top row) and AFM (bottom row) analysis, respectively.

3.2 Quantification of pOPN immobilized PAA-grafted BC

The concentration of pOPN adhered on the membrane was quantified by ELISA as describe earlier. A standard curve (**Figure 3.7**) which defined the relationship between the known concentration of pOPN (pg/ml) and optical density (OD) at 480 nm was used to calculate the remained pOPN after the immobilization step. The amount of initial pOPN (15.0 ng) was subtracted with the remained pOPN (0.33 ± 0.08 ng) to obtain the total pOPN that successfully bond to PAA-grafted BC (14.67 ± 0.08 ng) as show in **Table 3.4.** Furthermore, we found that the membrane was fully covered with pOPN approximately 3.86-7.72 ng/cm^2 and the PAA units provided an effective immobilization method for pOPN at highly 97 % immobilization efficiency [immobilization efficiency (%) = (total pOPN adhered on the membrane / initial pOPN) x 100]. In addition, it was reported by our research group previously that the amount of pOPN about 3.0-6.0 ng/cm^2 has a potential to induce cell adhesion and differentiation of mouse fibroblast (MC3T3). However, the maximum concentration of pOPN that can be immobilized on the PAA-grafted BC was not evaluated in this research and further study is required.

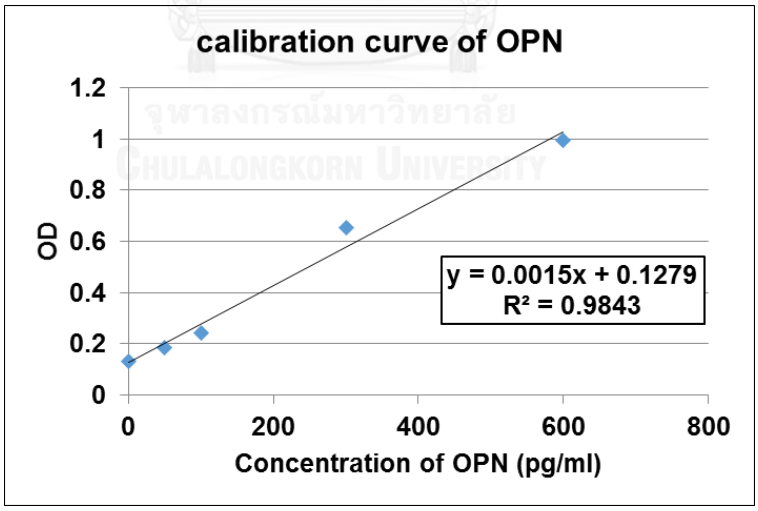

Figure 3.7. Calibration curve of pOPN quantified by ELISA

Table 3.4 Total amount of pOPN immobilized on the BC membrane quantified by ELISA

batch	remained pOPN after immobilization step			total pOPN adhered on the membrane	
	OD	(pg/mL)	(ng)	(ng)	Immobilization efficiency (%)
1	0.545	278.07	0.28	14.72	98.15
2	0.772	429.40	0.43	14.57	97.14
3	0.564	290.73	0.29	14.71	98.06
AV	0.630	332.73	0.33 ± 0.08	14.67 ± 0.08	97.78

3.3 Cytocompatibility Evaluation by MTT Assay

Following hPDLs seeding on the membranes for 24 hr., viable cells with active metabolism (NADH) directly convert MTT reagent into a purple formazan crystals inside cells near the cell surface. The quantity of formazan product detected at 540 nm serves as a useful marker which is presumably proportional to number of viable adherent cells on the membrane as shown in **Figure 3.8**. % cell viability of each samples were calculated using **Equation 2.1**. We found that amount of living cell on PAA-grafted BC immobilized with pOPN and rOPN (pOPN-BC and rOPN-BC) were slightly higher than those on both unmodified BC (BC) and PAA-grafted BC (PAA-BC). This information suggested that that the immobilized pOPN and rOPN can promote cell adhesion. However, no significant difference ($p > 0.05$) between all samples was found.

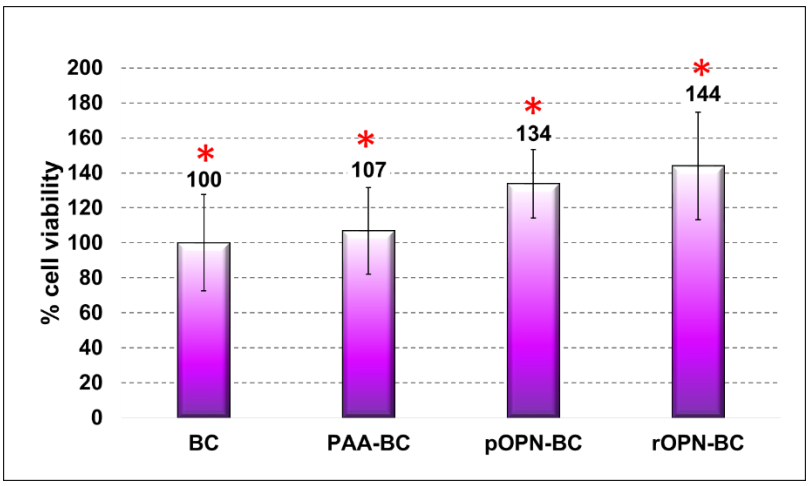

Figure 3.8 % Cell viability of hMSCs after cultured on unmodified BC (BC), PAA-BC, pOPN-BC, and rOPN for 24 hr (*p > 0.05).

3.4 Cellular adhesion of hPDLs

To investigate the biological function of pOPN immobilized PAA-grafted BC (pOPN-BC) for promoting cell adhesion of hPDLs in vitro, adherent cell morphology was observed follow immunofluorescent staining assay. The result was investigated in comparison with the cells cultured on the negative controls; untreated BC (BC) and PAA grafted-BC (PAA-BC), and the positive control; commercial recombinant OPN from HEX290 immobilized PAA-grafted BC (rOPN-BC). After 24 h of culture, the cells were fixed and treated with DAPI (blue) for nuclei staining follow by phalliodin-rhodamin [30] for actin filaments staining as shown in **Figure 3.9**. The staining pattern indicated that hPDLs could spread throughout the surface of both pOPN-BC and rOPN-BC better than on the control samples (BC and PAA-BC). Additionally, no distinct difference of cell morphology on pOPN-BC and rOPN-BC was found. These results represent the biocompatibility of pOPN-BC which is able to support hPDLs adhesion without an adverse effect on the cell morphology.

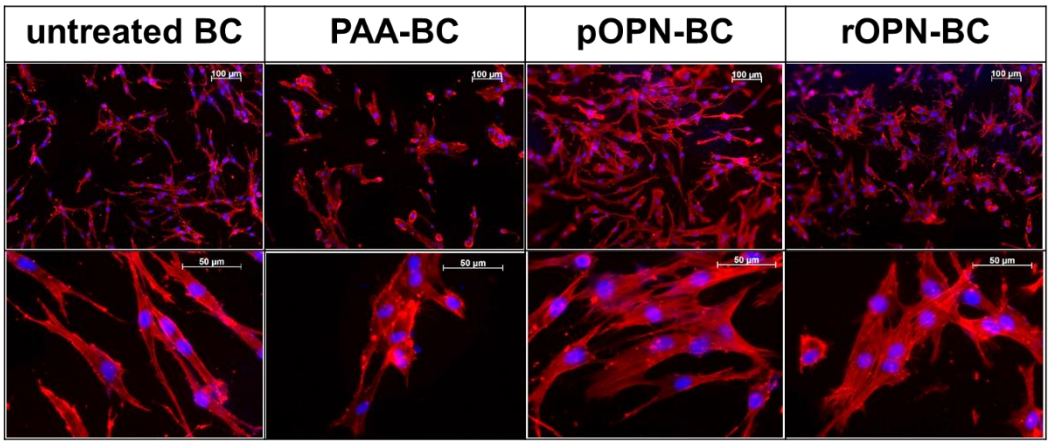

Figure 3.9 Immunofluorescent staining pattern of hPDLs adhered on unmodified BC (BC), PAA grafted-BC (PAA-BC), PAA grafted-BC immobilized with plant-derived OPN (pOPN-BC), and PAA-grafted BC immobilized with commercial recombinant OPN (rOPN-BC) [upper row : scale bar =100 µm (100X); lower row : scale bar =50 nm (400X)].

3.5 *In vitro* osteogenic differentiation of hMSCs by qPCR

To further confirm the potential of pOPN in bone tissue regeneration, we monitored the expression of some specific markers associated with osteogenic differentiation such as integrin-beta1 (ITGB1), Runt-related protein-2 (RUNX2), alkaline phosphatase (ALP), and collagen type 1 (COL1) after hPDLs was culture on the sample membranes in non-osteogenic medium for 1 and 3 days. All relative gene expression levels were normalized to the control samples (hPDLs cultured on unmodified BC; BC) as shown in **Figure 3.10.**The expression levels of osteogenic markers including ITGB1, RUNX2, ALP, and COL1 of pOPN and rOPN were relatively higher than those of control samples (BC). In contrast, ALP expression of pOPN (1D) was significantly higher than BC and rOPN-BC on Day 1 but subsequently decreased on Day 3 [pOPN (3D)]. These result need further study to explain the evidence. However, quantitative analysis of osteogenic markers by qPCR supported the results from immunofluorescent staining, which clarify the potential of pOPN-BC to promote osteogenic differentiation of hPDLs greater than BC alone.

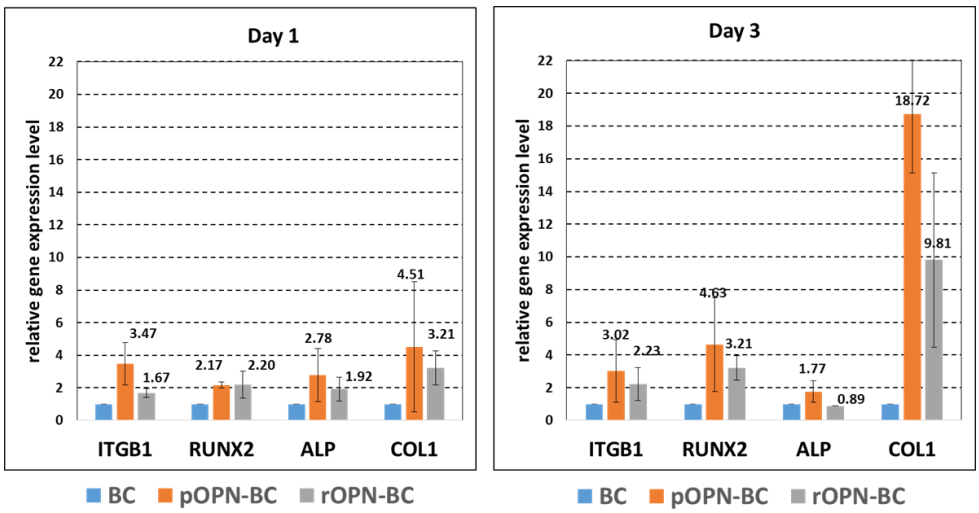

Figure 3.10 Relative gene expression levels examined by qPCR of osteogenic markers (ITGB1, RUNX2, ALP, and COL1) of hPDLs cultured on BC, pOPN-BC, and rOPN-BC in non-osteogenic medium after 1 day (A) and 3 days (B) were normalized to control samples (BC).

3.6 *In vitro* bone mineralization of hMSCs

To verify the potential of pOPN for promoting osteogenic differentiation, we observed mineralization process of hPDLs cultured on unmodified BC, pOPN-BC, and rOPN-BC using ARS assay. The more intense staining of Alizarin Red S in **Figure 3.11B** revealed the greater level of calcium deposition on pOPN-BC and rOPN-BC over the control sample (BC) after 11 days of culture. This result was further confirmed by quantitative measurement using CPC assay as display in **Figure 3.11A.** The dominant ARS levels of both pOPN-BC and rOPN-BC were higher than the control sample (BC) indicated that both recombinant OPN could support mineralization and osteogenic differentiation (*in vitro*) better than the culture on unmodified BC. Interestingly, due to the ARS levels of pOPN-BC that was significantly greater than rOPN-BC (p <0.05), we investigated the more efficacy of plant-produced OPN for supporting bone formation over the commercial rOPN. These results might be due to the difference in glycosylated pattern between pOPN and rOPN. This hypothesis will need further characterization of plant-produced OPN.

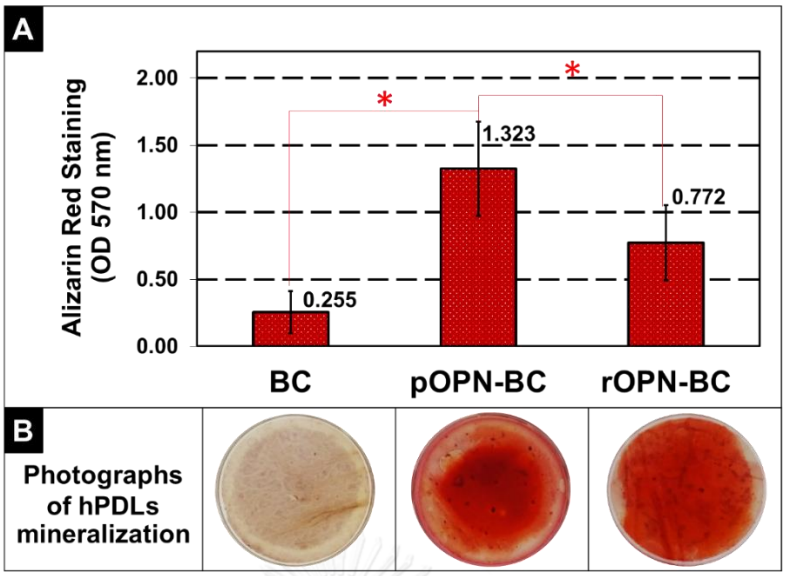

Figure 3.11 hPDLs mineralization on BC (control), pOPN-BC, and rOPN-BC after ARS staining. (A) graph represent quantity of ARS after elution by CPC assay (B) photographs show the extent of mineralization (*$p < 0.05$).

CHAPTER IV
CONCLUSION AND SUGGESTIONS

In this study, we demonstrated the success of grafting poly(acrylic acid) (PAA) brushes on BC membrane, and the presence of immobilized pOPN on the surface by ATR-FTIR and XPS analysis. PAA grafting via RAFT polymerization imposes no insignificant influence on mechanical strength and fibrous like structure of the BC. FE-SEM images revealed the fully coverage of accumulated round dot pOPN on the BC fibrils which was indirectly quantified as 3.86-7.72 ng/cm^2 by ELISA. Evidence from immunofluorescent staining, MTT assay, *in vitro* bone mineralization, and *in vitro* osteogenic differentiation of hMSCs by qPCR confirmed that the biological function of pOPN after surface immobilization was preserved to enhance bone tissue regeneration. Both of pOPN-BC and rOPN-BC potentially promote hPDLs adhesion and osteogenic differentiation greater than BC alone. Interestingly, we investigated the more efficacy of pOPN for supporting bone formation over the commercial rOPN that probably due to their both difference in glycosylated pattern during plant-produced process. Consequently, ours developed substrates may be clinically applied as a GTR membrane. However, its mechanism to promote regeneration and *in vivo* study is further required.

REFERENCES

[1] Zaborowska, M., Bodin, A., Backdahl, H., Popp, J., Goldstein, A., and Gatenholm, P. Microporous bacterial cellulose as a potential scaffold for bone regeneration. *Acta Biomater* **2010**, *6* (7), 2540-7.

[2] Garcia-Gareta, E., Coathup, M.J., and Blunn, G.W. Osteoinduction of bone grafting materials for bone repair and regeneration. *Bone* **2015**, *81*, 112-21.

[3] Dimitriou, R., Mataliotakis I, G., Calori Maria, G., and Giannoudis V, P. The role of barrier membranes for guided bone regeneration and restoration of large bone defects: current experimental and clinical evidence. *BMC medicine* **2012**, *10* (81), 2-24.

[4] Aurer, A. and JorgiÊ-Srdjak, K. Membranes for Periodontal Regeneration. *Acta Stomat Croat* **2005**, 107-112.

[5] Bruno Gasparini Betiatto de Sousa, et al. Analysis of tensile strength of poly(lactic-co-glycolic acid) (PLGA) membranes used for guided tissue regeneration. *RSBO* **2014**, *11* (1), 59-65.

[6] Zhang, Y., Zhang, X., Shi, B., and Miron, R. Membranes for guided tissue and bone regeneration. *annals of oral & maxillofacial surgery* **2013**, *1* (1), 1-10.

[7] Reiniati, I., Hrymak, A.N., and Margaritis, A. Recent developments in the production and applications of bacterial cellulose fibers and nanocrystals. *Crit Rev Biotechnol* **2017**, *37* (4), 510-524.

[8] Kwak, M.H., et al. Bacterial cellulose membrane produced by Acetobacter sp. A10 for burn wound dressing applications. *Carbohydrate Polymers* **2015**, *122*, 387-98.

[9] Kurniawan, H., Lai, J.-T., and Wang, M.-J. Biofuntionlized Bacterial Cellulose membranes by cold plasmas. *cellulose* **2012**, *19*, 1975-1988.

[10] Zhang, Y., Nypelö, T., Salas, C., Arboleda, J., Hoeger, I.C., and Rojas, O.J. Cellulose Nanofibrils. *Journal of Renewable Materials* **2013**, *1* (3), 195-211.

[11] Lin, N. and Dufresne, A. Nanocellulose in biomedicine: Current status and future prospect. *European Polymer Journal* **2014**, *59*, 302-325.

[12] Lee, S.H., et al. The effect of bacterial cellulose membrane compared with collagen membrane on guided bone regeneration. *Journal of Advanced Prosthodontics* **2015**, *7* (6), 484-95.

[13] Tazi, N., et al. Hydroxyapatite bioactivated bacterial cellulose promotes osteoblast growth and the formation of bone nodules. *AMB Express* **2012**, *2* (61), 1-10.

[14] Kirdponpattara, S., Khamkeaw, A., Sanchavanakit, N., Pavasant, P., and Phisalaphong, M. Structural modification and characterization of bacterial cellulose-alginate composite scaffolds for tissue engineering. *Carbohydrate Polymers* **2015**, *132*, 146-55.

[15] Ahn, S.-J., et al. Characterization of hydroxyapatite-coated bacterial cellulose scaffold for bone tissue engineering. *Biotechnology and Bioprocess Engineering* **2015**, *20* (5), 948-955.

[16] Gorgieva, S., Girandon, L., and Kokol, V. Mineralization potential of cellulose-nanofibrils reinforced gelatine scaffolds for promoted calcium deposition by mesenchymal stem cells. *Materials Science and Engineering: C Materials for Biological Applications* **2017**, *73*, 478-489.

[17] Lopes, T.D., Riegel-Vidotti, I.C., Grein, A., Tischer, C.A., and Faria-Tischer, P.C. Bacterial cellulose and hyaluronic acid hybrid membranes: Production and characterization. *International Journal of Biological Macromolecules* **2014**, *67*, 401-408.

[18] Wen, X., et al. Immobilization of collagen peptide on dialdehyde bacterial cellulose nanofibers via covalent bonds for tissue engineering and regeneration. *International Journal of Nanomedicine* **2015**, *10*, 4623-4637.

[19] Saska, S., et al. Bacterial cellulose-collagen nanocomposite for bone tissue engineering. *Journal of Materials Chemistry* **2012**, *22* (41), 22102-22112.

[20] Cho, H.J., et al. Effective immobilization of BMP-2 mediated by polydopamine coating on biodegradable nanofibers for enhanced in vivo bone formation. *ACS Applied Materials & Interfaces* **2014**, *6* (14), 11225-35.

[21] Martin, S.M., Ganapathy, R., Kim, T.K., Leach-Scampavia, D., Giachelli, C.M., and Ratner, B.D. Characterization and analysis of osteopontin-immobilized poly(2-hydroxyethyl methacrylate) surfaces. *Journal of Biomedical Materials Research Part A* **2003**, *67* (1), 334-343.

[22] Hao, C., Cui, Y., Owen, S., Li, W., Cheng, S., and Jiang, W.G. Human osteopontin: Potential clinical applications in cancer (Review). *International Journal of Molecular Medicine* **2017**, *39* (6), 1327-1337.

[23] Rangaswami, H., Bulbule, A., and Kundu, G.C. Osteopontin: role in cell signaling and cancer progression. *Trends in Cell Biology* **2006**, *16* (2), 79-87.

[24] Panda, D., et al. Potential roles of osteopontin and $\alpha_v\beta_3$ integrin in the development of coronary artery restenosis after angioplasty. *Proceedings of the National Academy of Sciences* **1997**, *94*, 9308–9313.

[25] Gadeau, A.-P., Campan, M., Dominique Millet, Candresse, T., and Desgranges, C. Osteopontin Overexpression is Associated with Arterial Smooth Muscle Cell Proliferation in Vitro. *Arteriosclerosis, Thrombosis, and Vascular Biology* 1993, *13*, 120-125.

[26] Kim, Y.-H., Jyoti, M.A., and Song, H.-Y. Immobilization of cross linked Col-I–OPN bone matrix protein on aminolysed PCL surfaces enhances initial biocompatibility of human adipogenic mesenchymal stem cells (hADMSC). *Applied Surface Science* **2014**, *303*, 97-106.

[27] Jensen, T., et al. Osteopontin functionalization of hydroxyapatite nanoparticles in a PDLLA matrix promotes bone formation. *Journal of Biomedical Materials Research Part A* **2011**, *99* (1), 94-101.

[28] Saito, K., Nakatomi, M., Ida-Yonemochi, H., and Ohshima, H. Osteopontin Is Essential for Type I Collagen Secretion in Reparative Dentin. *Journal of Dental Research* **2016**, *95* (9), 1034-1041.

[29] Rattanapisit, K.; Abdulheem, S.; Chaikeawkaew, D.; Kubera, A.; Mason, H.; Ma, J.; Pavasant, P. and Phoolcharoen, W. Recombinant human osteopontin expressed in Nicotiana benthamiana stimulates osteogenic related genes in human periodontal ligament cells. **2017**. Submitted.

[30] Dong, R., Krishnan, S., Baird, B.A., Lindau, M., and Ober, C.K. Patterned Biofunctional Poly(acrylic acid) Brushes on Silicon Surfaces. *Biomacromolecules* **2017**, *8*, 3082-3092.

[31] Seigel, R.R., Harder, P., Dahint, R., and Grunze, M. On-Line Detection of Nonspecific Protein Adsorption at Artificial Surfaces. *Analytical Chemistry* **1997**, *69* (16), 3321–3328.

[32] Chen, H. and Hsieh, Y.-L. Enzyme Immobilization on Ultrafine Cellulose Fibers via Poly(acrylic acid) Electrolyte Grafts. *biotechnology and bioengineering* **2005**, *90*, 405-413.

[33] Qu, Z., Hu, F., Chen, K., Duan, Z., Gu, H., and Xu, H. A facile route to the synthesis of spherical poly(acrylic acid) brushes via RAFT polymerization for high-capacity protein immobilization. *Journal of Colloid and Interface Science* **2013**, *398* , 82–87.

[34] Qu, Z., Chen, K., Gu, H., and Xu, H. Covalent immobilization of proteins on 3D poly(acrylic acid) brushes: mechanism study and a more effective and controllable process. *Bioconjugate Chemistry* **2014**, *25* (2), 370-378.

[35] Wen, F., et al. Induction of myogenic differentiation of human mesenchymal stem cells cultured on Notch agonist (Jagged-1) modified biodegradable scaffold surface. *ACS Appl Mater Interfaces* **2014**, *6* (3), 1652-1661.

[36] Sangsuwan, A., Narupai, B., Sae-ung, P., Rodtamai, S., Rodthongkum, N., and Hoven, V.P. Patterned Poly(acrylic acid) Brushes Containing Gold Nanoparticles for Peptide Detection by Surface-Assisted Laser Desorption/Ionization Mass Spectrometry. *Analytical Chemistry* **2015**, *87* (21), 10738-10746.

[37] Wanga, Y.-M., et al. Poly(Acrylic Acid) Brushes Pattern as a 3d Functional Biosensor Surface for Microchips. *Applied Surface Science* **2016**, *266*, 313–318.

[38] Steffensa, G.C.M., Nothdurfta, L., Busea, G., Thissen, H., Hockerb, H., and Kleeb, D. High density binding of proteins and peptides to poly(d,l-lactide) grafted with polyacrylic acid. *Biomaterials* **2002**, *23*, 3523–3531.

[39] Saxena, S., Ray, A.R., and Gupta, B. Chitosan immobilization on polyacrylic acid grafted polypropylene monofilament. *Carbohydrate Polymers* **2010**, *82* (4), 1315-1322.

[40] Thomas, D.B., et al. Kinetics and Molecular Weight Control of the Polymerization of Acrylamide via RAFT. *Macromolecules* **2004**, *37*, 8941-8950.

[41] Semsarilar, M. and Perrier, S. 'Green' reversible addition-fragmentation chain-transfer (RAFT) polymerization. *Nature Chemistry* **2010**, *2* (10), 811-20.

[42] Sharpe, P.T. Dental mesenchymal stem cells. Development 143(13) (2016): 2273-80.

[43] Osathanon, T., Ritprajak, P., Nowwarote, N., Manokawinchoke, J., Giachelli, C., and Pavasant, P. Surface-bound orientated Jagged-1 enhances osteogenic differentiation of human periodontal ligament-derived mesenchymal stem cells. *Journal of Biomedical Materials Research Part A* **2013**, *101* (2), 358-67.

[44] Ullah, I., Subbarao, R.B., and Rho, G.J. Human mesenchymal stem cells - current trends and future prospective. *Bioscience Reports* **2015**, *35* (2), 1-18.

[45] Svensson, A., et al. Bacterial cellulose as a potential scaffold for tissue engineering of cartilage. *Biomaterials* **2005**, *26* (4), 419-431.

APPENDIX

VITA

Miss Nichapa Klinthoopthamrong was born in 20th February, 1992 in Ayuthtaya, Thailand. She graduated a Bachelor's Degree of Science with a second-class honors from Department of Chemistry, Faculty of Science and Technology, Thammasat University, Thailand in 2014. After that, in the same year, she started to enroll as a Master Degree student of Program in Petrochemistry and Polymer Science, Faculty of Science, Chulalongkorn University. All of her research work was carried out at Oraganic Synthesis Research Unit (OSRU), Department of Chemistry, Faculty of Science, Chulalongkorn University and she graduated her academic in July, 2017.

Proceeding:

Poster presentation was performed at the 23th PPC Symposium on Petroleum, Petrochemicals and Polymers and 8th Research Symposium on Petrochemical and Materials Technology Conference, Pathumwan Princess Hotel, Bangkok, Thailand. (May 23th, 2017)